Classification
Physics Abstracts
61.30 — 64.70 — 82.70

Local structures of the surfactant aggregates in dilute solutions deduced from small angle neutron scattering patterns

J. Marignan (1), J. Appell (1), P. Bassereau (1), G. Porte (1) and R. P. May (2)

(1) Groupe de Dynamique des Phases Condensées (associated to the C.N.R.S. UA 233), Université des Sciences et Techniques du Languedoc, 34060 Montpellier, France
(2) Institut Max von Laue-Paul Langevin, BP 156X, 38042 Grenoble, France

(*Reçu le 5 mai 1989, révisé le 24 juillet 1989, accepté le 31 août 1989*)

Résumé. — Nous étudions par diffusion des neutrons aux petits angles (vecteur de diffusion compris entre 2×10^{-3} et 5×10^{-1} Å^{-1}) les trois structures locales (sphère, cylindre, plan). Nous avions précédemment montré [1, 8, 9] de façon indirecte que les agrégats de surfactants adoptaient l'une ou l'autre de ces trois structures dans les phases riche en eau (salée) de systèmes binaires (surfactant/eau salée) ou ternaires (surfactant/eau salée/hexanol). Nous obtenons une confirmation directe de ces structures et déterminons avec précision leurs dimensions caractéristiques.

Abstract. — The three local structures (spherical, cylindrical and planar) previously assumed [1, 8, 9] to be that of the surfactant aggregates in the brine rich phases of binary (surfactant-brine) or ternary (surfactant-alcohol-brine) are studied by small angle neutron scattering (scattering vectors range from 2×10^{-3} to 5×10^{-1} Å^{-1}). We confirm entirely the previous assumptions and determine precisely the characteristic dimensions for these structures.

1. Introduction.

In the recent years two of the phases formed in solutions of surfactants have received increasing attention namely the solutions of large elongated micelles and the so-called anomalous isotropic phase (L_3).

Large elongated micelles have been studied in dilute solutions where they offer an example of unidimensional growth [1-3] : they are pictured as long flexible cylinders and they are thus expected to display polymer-like behavior. In semi dilute solutions, Candau *et al.* [4] indeed found typical scaling law behaviors (for scattered light intensity, diffusion coefficient, etc.). These polymer-like micelles offer a further opportunity namely they exist with a large distribution of lengths in dynamical equilibrium and are thus « living polymers » [5] which are expected to display peculiar rheological properties. All these studies imply a flexible cylindrical local structure characterized by the radius of the cylinder and by a persistence length which is a measure of the flexibility. Clearly the relative magnitude of this length with

respect to the radius is crucial for the validity of the polymer-like representation of elongated micelles.

The anomalous isotropic phase L_3 is encountered in many systems (non-ionic surfactant in water, ionic surfactant plus alcohol in brine...). It is optically isotropic at rest but exhibits striking birefringence upon shaking. Recent studies [6, 7] suggest a bicontinuous phase with an infinite bilayer separating two interwoven selfconnected brine domains. In this picture, the bilayer is a film with the same topology as the monolayer film separating the oil and water domains in a bicontinuous microemulsion. In the L_3 phase the two disconnected domains are identical and the film has a spontaneous curvature equal to zero ; this is not the case anymore in the bicontinuous microemulsion where the asymmetry of the domains can introduce a finite spontaneous curvature. The L_3 phase thus represents a « simplified » model for bicontinuous microemulsion, to test different structural descriptions. This implies that the local structure of the surfactant aggregates is a thin bilayer (of very small thickness compared to its extension).

For some time, we have been engaged in the detailed study of the phases formed in some water (or brine) rich binary (surfactant/water) or ternary (surfactant/alcohol/water) systems. We showed that the polymorphism was rich in these systems [1, 8, 9] in agreement with other groups' work [3, 10, 11] and tried to understand the phase behavior in terms of the morphological transformations of the elementary objects induced by addition of salt to the binary systems [2] or by the variation of the alcohol-to-surfactant ratio in the ternary system [12]. The local structure of the elementary objects was infered from the nature of the observed phases (micellar solutions, lamellar lyotropic liquid crystal L_α and anomalous isotropic phase L_3) and from more or less indirect experimental evidences [1, 8, 9]. We found the, now classical, sequence for the local structure of aggregates due to the self-assembly of surfactants plus (in some cases) alcohol molecules, namely spherical, cylindrical and planar structures. A low spatial resolution small-angle neutron scattering study [9] confirmed the previous assumptions, however an exact quantitative assessment of characteristic dimensions is impeded by the possible existence of interaggregates interactions which, although weak, can modify the scattering pattern.

The purpose of the present study is to confirm our previous results and to obtain exact quantitative values of the characteristic dimensions of the three local structures which, as stated above, are prerequisites to the use of the surfactant phases as model systems. In order to reach our goal we first choose appropriate samples representative of the three local structures amenable to a small-angle neutron scattering study on the largest possible q-range and in particular with the highest spatial resolution. The scattering patterns are then analysed using the well established procedures for the structural studies of colloidal or micellar aggregates [13-15].

In the successive parts of the paper we discuss in turn the results on each local structure, namely spherical, cylindrical or planar. We indicate the nature of the chosen samples and then describe and analyze the scattering pattern.

2. Experimental.

2.1 SAMPLE PREPARATION. — Cetylpyridinium bromide (CPBr), cetylpyridinium chloride (CPCl), hexanol and sodium bromide and chloride are the same as in [8]. Deuterated brine were prepared by dissolution of the salts in D_2O (99.8 % D). The samples were prepared by weight.

2.2 SMALL ANGLE NEUTRON SCATTERING : DATA ACQUISITION AND TREATMENT. — The small angle neutron scattering experiments are performed at the cameras D11 and D16 of the

Institut Laue Langevin in Grenoble. The samples are contained in quartz cells (Hellma) (with a path of 2 mm). An area of 1 cm^2 is illuminated by the neutron beam. Intensities relative to the incoherent scattering of H_2O in a cell with a path of 1 mm are obtained from the measured intensities after substraction of the solvent and empty cell contributions. The data are then handled according to standard procedures [16, 17]. Only one contrast factor is assumed : the contrast is mainly between the hydrogen atoms of the aggregates and the deuterium atoms of the solvent [15]. The density (ρ) of the surfactant in the aggregates is derived from the evolution of the binary surfactant brine mixture as a function of solvent volume fraction (linear dependence) giving for CPCl ($\rho = 0.96$ g/cm^3) and for CPBr ($\rho = 1.07$ g/cm^3) and the density of hexanol in the aggregates is assumed to be that of the pure liquid hexanol ($\rho = 0.82$ g/cm^3). The fast exchange between the initially protonated OH groups of the hexanol and the deuterium atoms of the brine solvent is taken into account (this is certainly important in the estimation of the mass of the aggregates).

At D11, experiments are performed with low spatial resolution ; the wavelength = 10 Å and the scattering vectors (q) range from 2×10^{-3} Å^{-1} to 1.5×10^{-1} Å^{-1}. In this q-range interactions between aggregates can show up in the scattering pattern, however we studied very diluted samples ($\leqslant 1$ % aggregates) and neglected eventual interactions in our treatment of the data. The excellent agreement found between the geometrical characteristics derived from these measurements and from the measurements at D16 indicates that this neglect is reasonable.

At D16, the experiments are performed with high spatial resolution ; the wavelength = 4.52 Å and the scattering vectors (q) range from 7×10^{-2} Å^{-1} to 5×10^{-1} Å^{-1}. We computed the invariant Q and the ratio of surface to volume (s/v) [13-15] :

$$Q = \int_0^\infty q^2 I(q)\, dq \qquad \text{and} \qquad \frac{s}{v} = \frac{\pi}{Q} \lim_{q \to 0} [q^4 I(q)] . \tag{1}$$

For a disordered material and in the large-q limit the interactions between aggregates have no influence on the scattering pattern which reflects only the local structure and we studied more concentrated samples in order to increase the scattering cross-sections. The values obtained for the invariants and the Porod limits are given, in table I, for the three studied samples.

Table I. — *The invariant Q and the Porod limit obtained for the three samples.*

Sample	Q cf. (1) (cm^{-4})	$\lim_{q \to 0} [q^4 I(q)]$ (cm^{-5})
CPCl 0.05 g/cm^3 + 0.2 M NaCl sphere	9.2×10^{27}	2.5×10^{21}
CPBr 0.05 g/cm^3 + 0.8 M NaBr cylinder	8.9×10^{27}	2.85×10^{21}
CPCl 0.043 g/cm^3 + Hexanol 0.047 g/cm^3 + 0.2 M NaCl planar	2.3×10^{28}	7.7×10^{21}

2.3 LIGHT SCATTERING. — In one case we completed the scattering pattern at low q by measuring the angular distribution of scattered light on the laboratory set up : the light source is an argon ion laser working at 4 880 Å, the beam is focalised on the sample contained in a cylindrical cell and the scattered photons are collected on a photon multiplier and counted as a function of scattering angle. The scattering vectors q range from 3×10^{-4} Å^{-1} to 3×10^{-3} Å^{-1}.

3. Globular structure.

The studied samples are two micellar solutions : 0.01 g/cm^3 CPCl (at low q's) and 0.05 g/cm^3 CPCl (at larger q's) in 0.2 M NaCl brine. From previous studies the micelles are expected to be globular [18, 19].

3.1 LOW q SCATTERING PATTERN. — If the local structure is globular we expect the scattered intensity to vary as [13-15]

$$I(q) = cM(b_m - v_m \rho_0)^2 \exp(-R_g^2 q^2/3) \qquad (2)$$

at small q ($qR_g \leqslant 1$). R_g is the radius of gyration of the particle, c is the concentration (g/cm^3), M is the mass of the particle (g), and $(b_m - v_m \rho_0)$ is the contrast difference [20] between the particle and the solvent (cm/g).

In figure 1, Ln $(I(q))$ is plotted as a function of q^2. From the linear part at the lowest q's, we compute using (2) : from the slope, $R_g = 20 \pm 2$ Å and from the extapolated intensity $I(0)$, $M = (6.6 \pm 0.5) \times 10^{-20}$ g. Assuming the aggregates to be perfect spheres ($r_g^2 = \frac{5}{3} R_g^2$ and $r_m^3 = \frac{3M}{4\pi\rho}$) we obtain two estimates of their radius :

$$r_g = 26 \pm 2 \text{ Å} \qquad \text{and} \qquad r_m = 25.5 \pm 4 \text{ Å} .$$

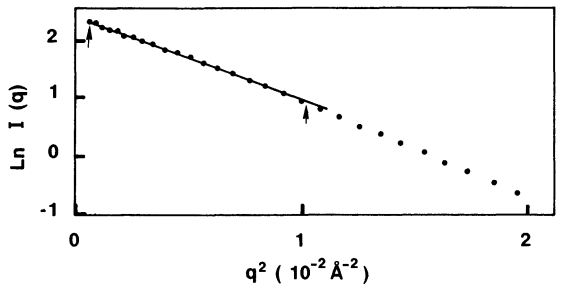

Fig. 1. — Guinier plot Log $(I(q))$ *vs.* q^2 for the sample 1 % CPCl in 0.2 M NaCl brine representative of the spherical local structure. The arrows indicate the limits : $qR_g = 0.2$ and 2 between which (2) is found to hold.

3.2 LARGE q SCATTERING PATTERN. — From the Porod limit using (1) and assuming the micelles to be perfect monodisperse spheres we obtain another estimate of the radius of the sphere :

$$r_p = 26 \pm 4 \text{ Å} .$$

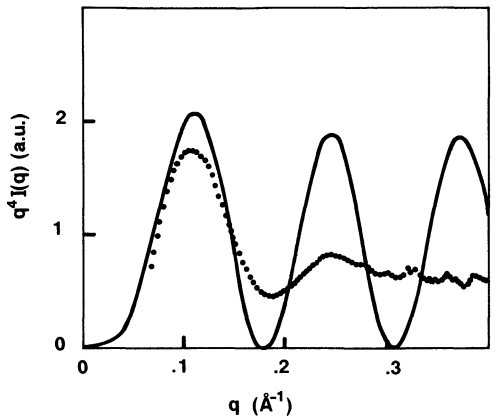

Fig. 2. — Form factor oscillations in the Porod region. The full line = calculation for spheres with $r = 25$ Å ; dots = experimental result for the sample : 5 % CPCl in 0.2 M NaCl brine.

As usual, oscillations reflecting the form factor of the scattering objects are observed in the plot of $q^4 I(q)$ *versus* q shown in figure 2. Assuming, as previously, that the micelles are spheres :

$$I(q) \propto \left[3 \frac{\sin (qr) - qr \cos (qr)}{(qr)^3} \right]^2 \tag{3}$$

the form factors corresponding to different radii r are computed and compared to the experimentally observed oscillations. We seek for the best agreement for the position of the extrema : this is found to be very sensitive to the chosen radius. In figure 2 the curve computed with $r = 25$ Å is displayed, the agreement is good for the position of the three first extrema and is the best we observed (trials with the form factors for a cylinder (4) or a plane (9) led to no agreement). We thus obtain a fourth estimate of the radius of the sphere : $r_0 = 25 \pm 1$ Å. The experimental damping of the oscillations can be due to a size polydispersity and/or to a small shape anisometry of the micelles. Looking carefully at figure 2 we note that, although the overall agreement between calculated and experimental extrema is good, the first experimental maximum is on the left of the calculated one, the first experimental minimum is on the right and the second maximum matches exactly. If the damping was due to polydispersity alone we would not expect such deviations from the exact positions of the extrema, which would correspond to a mean radius. On the contrary, a shape anisometry of the micelles could explain both the damping and the deviation from exact coincidences of the extrema. These experimental results are thus in favor of a small anisometry of the micelles, too small, however to be quantitatively established.

The evidences obtained at all q's are in excellent agreement with one another and confirm that the small micelles have a quasi-spherical form. The four estimates obtained for the radius of the globular micelles are equal within experimental errors (cf. Tab. II) $r = 25 \pm 1$ Å. It is interesting to compare the radius thus obtained to the average hydrodynamic radius of the CPCl micelles previously obtained by quasi-elastic light scattering [18] : $R_h = 29 \pm 2$ Å. The agreement is good if one recalls that R_h measures the radius of the equivalent diffusing sphere (micelle + hydration layer) while the r's measured here are the radius of the dry equivalent spheres (the hydration layer has no contrast with respect to the free solvent).

Table II. — *The radius of the spherical local structure : the micelles of* CPCl *in* 0.2 M NaCl *brine.*

Method of determination	Radius (Å)
$I(q)$ Guinier plot in the low q-range :	
from the radius of gyration R_g	26 ± 2 Å
from the mass M	25.5 ± 4 Å
S/V ratio from the Porod limit	26 ± 4 Å
From the positions of the extrema of the oscillations in the Porod region	25 ± 1 Å

4. Cylindrical structure.

The studied samples are two micellar solutions : 0.01 g/cm^3 CPBr (at low q's) and 0.05 g/cm^3 CPBr (at larger q's) in 0.8 M NaBr brine. From previous studies the micelles are expected to be large flexible cylinders [1, 18, 19].

4.1 LARGE q SCATTERING PATTERN. — From the Porod limit using (1) and assuming the micelles to be long rods with a circular cross-section we obtain an estimate of the cross-sectional radius :

$$r_p = 20.5 \pm 4 \text{ Å} .$$

Oscillations reflecting the form factor of the scattering objects are observed in the plot of $q^4 I(q)$ *versus* q shown in figure 3. Assuming that the micelles are cylinders :

$$I(q) \propto \frac{1}{q} \left[2 \frac{J_1(qr)^2}{(qr)} \right]^2 \tag{4}$$

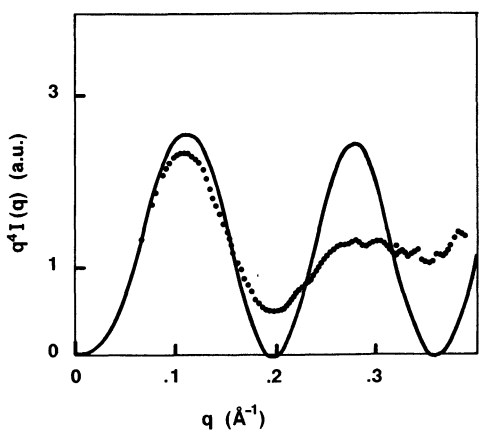

Fig. 3. — Form factor oscillations in the Porod region. The full line = calculation for cylinders with a circular cross section r = 19.5 Å ; dots = experimental result for the sample : 5 % CPBr in 0.8 M NaBr brine.

the form-factor for cylinders of different radius r is computed and compared to the experimentally observed oscillations. We seek for the best agreement for the position of the extrema. In figure 3 we compare our data with the curve computed for $r = 19.5$ Å, the coincidence in position of the three experimental and computed extrema is found to be very sensitive to the chosen radius (the precision is probably better than 0.5 Å) ; here again trials with the form-factors for other structures (sphere (3) or plane (9)) led to no agreement. We thus obtain another estimate of the radius of the cylinder : $r_0 = 19.5 \pm 1$ Å. The observed experimental damping of the oscillations (see Fig. 3) can be due to fluctuations of the radius of the cylindrical micelles and/or to a small ellipticity of their cross-section. We have no clue allowing to choose between these possibilities.

4.2 LOW q SCATTERING PATTERN INCLUDING LIGHT SCATTERING DATA. — In figure 4 the neutron and light scattering patterns are displayed illustrating the excellent overlap between the two patterns (within a scaling factor). In this log/log representation, two linear regions can clearly be distinguished the first one at the lowest q's has a zero slope and corresponds to the overall finite size of objects and the second one in the intermediate q-range with a slope equal to one is indicative of rod-like objects [15].

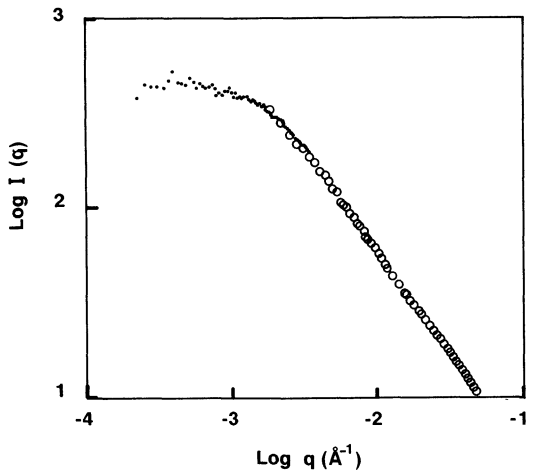

Fig. 4. — Log/Log display of the low q-range spectral pattern. (•) = light scattering and (○) = neutron scattering for the sample 1 % CPBr in 0.8 M NaBr brine representative of the cylindrical local structure.

4.3 INTERMEDIATE q-RANGE : THE RADIUS OF THE CYLINDER. — For a random distribution of rod-like particles we expect $qI(q)$ to vary as [13, 14] :

$$qI(q) = \pi c M_L (b_m - v_m \rho_0)^2 \exp(-R_c^2 q^2/2) \qquad (5)$$

in the range $qR_c < 1$ and $q\langle \ell \rangle \geqslant 1$ where R_c is the radius of gyration of the normal section of the rod and $\langle \ell \rangle$ is the persistence length i.e. the average length below which the linear object can be considered as straight and rigid ; in figure 4 a q-range where $I(q) \propto q^{-1}$ is indeed observed (see above). In (5) M_L is the mass per unit length of the rod. Ln $(qI(q))$ as a function of q^2 is shown in figure 5. From the linear dependence in the range 3×10^{-2} Å$^{-1} < q < 1.5 \times 10^{-1}$ Å^{-1} we deduce using (3) : $R_c = 15.5 \pm 2$ Å and $M_L = [1.6 \pm 0.2] \times 10^{-13}$ g/cm. From these values, assuming that the rod has a circular cross-section

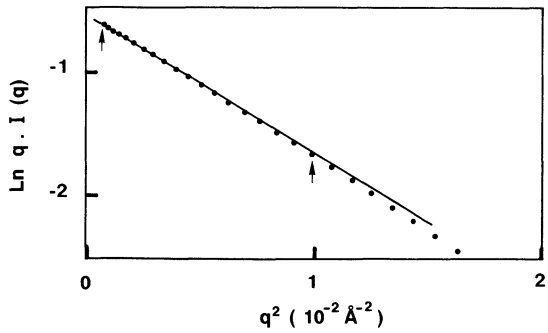

Fig. 5. — Log($qI(q)$) as a function of q^2 in the intermediate low q-range for the sample 1 % CPBr in 0.8 M NaBr brine. The arrows indicate the limits : $qR_c = 0.4$ and 1.5 between which (5) is found to hold.

($r_g^2 = 2\,R_c^2$ and $r_m^2 = \dfrac{M_L}{\pi\rho}$), we obtain two estimates of its radius : $r_g = 22 \pm 2$ Å and $r_m = 22 \pm 4$ Å.

4.4 LOWER q-RANGE : EVIDENCE FOR THE FLEXIBILITY OF THE LONG CYLINDRICAL MICELLES. — We stated above that (5) is valid down to q's such $q\langle\ell\rangle \geqslant 1$ so that if the objects are infinite rigid cylinders (5) will be valid down to $q = 0$ while, if they are rigid cylinders of finite length L, $[qI(q)]$ will fall to zero with q from $q \approx (L^{-1})$ downwards. A plot of $qI(q)$ *versus* q in the lowest q-range is shown in figure 6 ; clearly instead of one of the two behaviors expected for rigid cylinders a third behavior is observed : going downwards along the q-axis (5) is valid down to $q \approx 1.5 \times 10^{-2}$ Å^{-1}, $qI(q)$ then increases before falling down to zero. This last behavior indicates that the scattering objects have a finite size (see below).

Let us first examine the possible origin of this bump in the $qI(q)$ plot. Such an upward trend has already been previously observed in the neutron scattering spectra of another micellar system [21], but was then interpreted as the indication of a secondary aggregation of the micelles. However we suspect from our previous studies [18, 22] that the long rod-like micelles are flexible cylinders and we feel that the upward trend in the $qI(q)$ plot could be due to this flexibility. The asymptotic limit of $I(q)$ goes over from q^{-1} in the case of a long thin rod (cf. (5)) to q^{-2} for a Gaussian coil [23] ; in the intermediate case of a flexible rod, the two dependences of $I(q)$ with q must be observable in two adjacent ranges of q provided they are not obscured by the exponential decays, due to the finite radius of the cross section of the rods on the highest q side and to the finite size of the flexible coil on the lowest q side. Such a cross over from one dependence to the other of $I(q)$ on q occurs at [24] $q_c \approx 1.9/\langle\ell\rangle$, from figure 6 we can estimate $q_c \approx 1 \times 10^{-2}$ Å^{-1}. We thus obtain for the persistence length $\langle\ell\rangle = 190 \pm 50$ Å. If our attribution of the upward trend to the influence of the flexibility on the scattering pattern is correct the following relation [25] should furthermore hold :

$$qI(q) \to \frac{\pi}{L_{cyl}} + \frac{2}{3\langle\ell\rangle\, L_{cyl}\, q} \tag{6}$$

for $L_{cyl}^{-1} \ll q \ll R_c$ with L_{cyl} the length of the flexible cylinders. The plot of $qI(q)$ *versus* q^{-1} is shown in figure 7 in the appropriate q-range ; this plot is approximately linear and from its slope and origine we can deduce another estimate of $\langle\ell\rangle = 180 \pm 50$ Å. We had previously obtained other estimates of $\langle\ell\rangle$ by two entirely different methods [19, 22] (relative evolution of overall radius of gyration and hydrodynamic radius measured in light scaterring

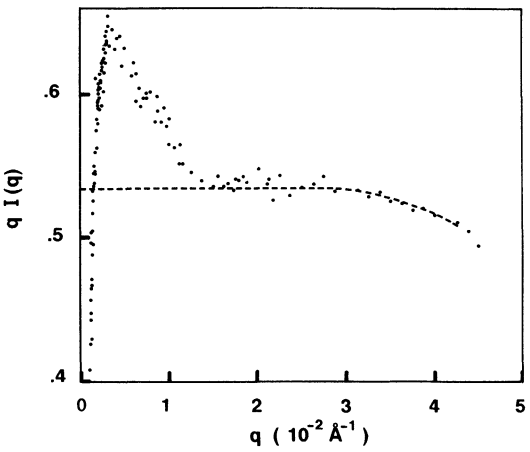

Fig. 6.

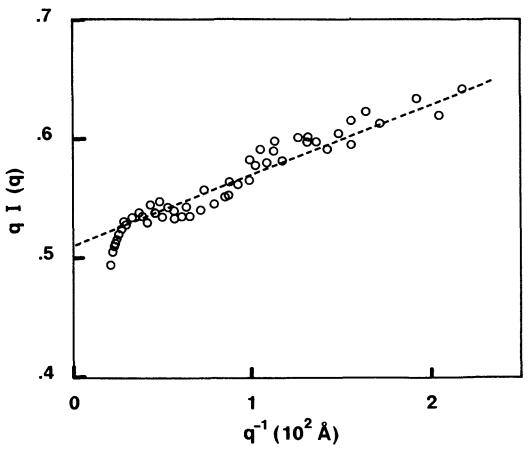

Fig. 7.

Fig. 6. — Manifestation of the flexibility of the cylinders in the $qI(q)$ plot for the sample 1 % CPBr in 0.8 M NaBr brine (see text).

Fig. 7. — Approximately linear part of $qI(q)$ as a function of q^{-1} which allows for the determination of the persistence length characteristic of the flexibility of the cylinders for the sample 1 % CPBr in 0.8 M NaBr brine (see text).

experiments and magnetic birefringence experiments) ; with these methods we had to take into account explicitly the size distribution of the micelles in the experimental situations so that the estimates of $\langle \ell \rangle$ were somewhat dependent on the model of micellar growth assumed. The estimated $\langle \ell \rangle \approx 200 \pm 50$ Å is however in excellent agreement with the present values. In the present procedure, we neglect the interference effects due to interactions between scattering objects which could modify the scattering pattern due to the « single » object in the present q-range. The hight salinity of the sample which insures an efficient screening of the long range electrostatic interactions is a partial justification for this neglect which is further justified by the good agreement between the different estimates of $\langle \ell \rangle$.

4.5 THE LOWEST q-RANGE. — Drawing an analogy between the long, flexible, cylindrical micelles and polymers, we expect in this range, to gain information either on the overall size reflected by the radius of gyration of the coil if the solution is dilute or on the correlation length ℓ_c which is a measure of the mean distance between the entanglements of the polymer chains if the solution is semi-dilute [26]. The situation is here complicated by the fact that the long micelles are expected [1] to have a very broad size distribution so that possibly the largest micelles form an entangled network while the smallest ones are still free in the meshes of this network. For free coils we expect $I(q)_{q \to 0} \propto \exp(-q^2 R_g^2/3)$ (with R_g the mean radius of gyration). For entangled coils the Ornstein-Zernicke expression reduces to $I(q)_{q \to 0} \propto \exp(-q^2 \ell_c^2)$ for $q\ell_c \ll 1$. Our purpose here is not to make a precise measurement but to evaluate an order of magnitude of a length ξ which is possibly some combination of $\xi = R_g/\sqrt{3}$ and $\xi = \ell_c$ and to compare this length to the previously determined persistence length $\langle \ell \rangle$. This length ξ is determined assuming

$$I(q)_{q \to 0} \approx \exp(-q^2 \xi^2) \tag{7}$$

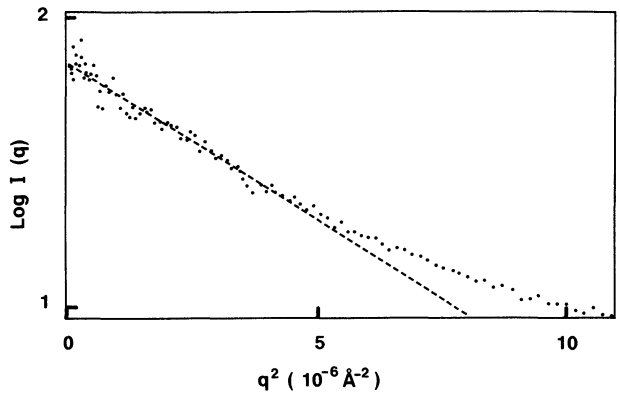

Fig. 8. — Guinier plot Log $I(q)$ *vs.* q^2 in the lowest q-range (light scattering) for the sample 1 % CPBr in 0.8 M NaBr brine.

ξ is deduced from the slope at the origin of the Guinier plot shown in figure 8. We obtain $\xi = 900 \pm 100$ Å. If we interpret this value as $\xi = R_g/\sqrt{3}$ we obtain a fairly small value of R_g(~ 500 Å); in our previous investigations [18, 22] on more dilute solutions of CPBr in 0.8 M NaBr brine we had evidence that the micelles had already larger mean radius of gyration so that the interpretation of ξ as a correlation length or eventually as some mean between a correlation length and radiis of gyration seems appropriate.

The results obtained on these elongated micelles at all scales thus lead to the following picture : the micelles are long flexible cylindrical micelles, the radius of the cross section of the cylinders is $r = 19.5 \pm 1$ Å, and the persistence length, characteristic of their flexibility, is equal to 180 ± 50 Å. We note that the radiis determined from the Guinier plot in the intermediate q-range which reflects the cylindrical structure are larger (22 Å) than the radius (19.5 Å) deduced from the form factor oscillations at large q (cf. Tab. III) ; this can well be

Table III. — *The radius of the cylindrical local structure : the micelles of* CPBr *in* 0.8 M NaBr *brine.*

Method of determination	Radius r (Å)
$qI(q)$ Guinier plot in the low q-range : from the radius of gyration R_g from the mass/unit length M_L	 22 ± 2 Å 22 ± 4 Å
S/V ratio from the Porod limit	20.5 ± 4 Å
From the positions of the extrema of the oscillations in the Porod region	19.5 ± 1 Å

due to the fact that the cylinders are flexible on a scale which is not much larger than their diameter (180 Å compared to 40 Å) and that the influence of this flexibility on the scattering pattern can already be perceptible in the intermediate q-range. On the other hand the persistence length characteristic of the flexibility is not very much smaller than the correlation length ξ deduced from the lowest q-range. This restricts severely the q-range where the influence of the flexibility of the coils is perceptible and from which we deduced the value of this persistence length. However as already stated the good agreement between values obtained from very different experiments reinforces our interpretation although it would be preferable to find tractable experimental situations where the cylindrical micelles would be longer and in a dilute solution.

5. Planar structure.

Two samples of the L_3 phase (anomalous isotropic phase) of the CPCl-hexanol-0.2 M NaCl brine system [8] have been studied with a ratio hexanol/CPCl = 1.1 in weight and 91 % brine (large q's) and 97.7 % brine (at lower q's). In previous studies [7, 9] we have obtained strong evidence for a bilayer structure on a local scale and no long range order.

5.1 LOW-q SCATTERING PATTERN. — For a random distribution of large flat particles we expect $q^2 I(q)$ to vary as [13, 14]

$$q^2 I(q) = 2\pi^2 c M_A (b_m - v_m \rho_0)^2 \exp(-d_g^2 q^2/12) \qquad (8)$$

in the range $qd_g < 1$ and $q > L^{-1}$ where d_g is the apparent dry thickness of the bilayer (as derived [13, 14] from the one dimensional radius of gyration of the scattering length density along the normal to the bilayer) and L is a dimension characteristic of the lateral extension of the flat bilayer ; M_A is the mass per unit area of the bilayer. In figure 9 a logarithmic plot of $q^2 I(q)$ is shown : in the lowest q range a linear variation corresponds to (8) and we derive from its slope $d_g = 24 \pm 2$ Å and from its extrapolation to $q = 0$, $M_A = [2.1 \pm 0.1] \times 10^{-7}$ g/cm^2 from which assuming a constant thickness of the bilayer ($d_m = M_A/\rho$) we derive $d_m = 23 \pm 4$ Å in good agreement with the value d_g.

5.2 LARGE-q SCATTERING PATTERN. — From the Porod limit using (1) and assuming here again a flat local structure we obtain an other estimate of the thickness of the bilayer $d_p = 22 \pm 4$ Å.

Oscillations reflecting the form factor of the scattering objects are observed in the plot of

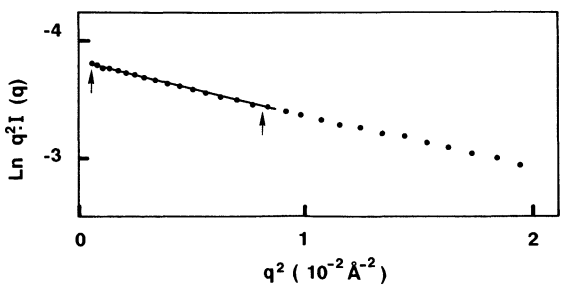

Fig. 9. — Log($q^2 I(q)$) *vs.* q^2 in the low q-range for the sample CPCl + hexanol in 0.2 M NaCl brine (97.7 % Brine). This sample is representative of the planar local structure. The arrows indicate the limits $qd_g = 0.5$ and 2 between which (8) is found to hold.

$q^4 I(q)$ *versus* q shown in figure 10. Assuming that the scattering objects are bilayers :

$$I(q) \propto \frac{1}{q^2} \left[\frac{\sin (qd/2)}{(qd/2)} \right]^2 \tag{9}$$

the intensity scattered by bilayers of different thicknesses d is computed and compared to the experimentally observed oscillations. The best agreement for the position of the extrema in the calculated and experimental curves is obtained for $d_0 = 22 \pm 1$ Å. The coincidence in position of the two experimental and computed extrema is found to be very sensitive to the chosen thickness ; here again trials with the form factors for other structures (sphere (3) or cylinder (4)) led to no agreement. The fluctuations of the thickness of the bilayers must be responsible for the observed experimental damping of the oscillations (see Fig. 10).

The evidences obtained at all q's in excellent agreement with one another and they totally confirm the assumed [7, 9] local structure in the L_3 phase : a planar bilayer. The four estimates obtained for the thickness of the bilayer are in reasonable agreement (cf. Tab. IV) ;

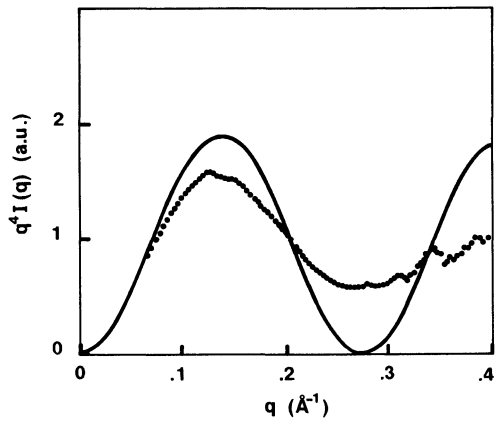

Fig. 10. — Form factor oscillations in the Porod region. The full line = calculation for flat bilayers with $d = 22$ Å ; dots = experimental result for the sample : CPCl + hexanol in 0.2 M NaCl brine (90 % brine).

Table IV. — *The thickness of the planar local structure :* L_3 *in the* CPCL-*hexanol*-0.2 M NaCl *brine system.*

Method of determination	Thickness d (Å)
q^2 $I(q)$ Guinier plot in the low q-range :	
from the radius of gyration	24 ± 2 Å
from the mass/unit area M_A	23 ± 4 Å
S/V ratio from the Porod limit	22 ± 4 Å
From the positions of the extrema of the oscillations in the Porod region	22 ± 1 Å

the somewhat larger values obtained from the lower q-range pattern is possibly due to the fact that the bilayers are not completely rigid at this scale (as assumed in (8)) and that the influence of their flexibility is perceptible in the scattering pattern in this q-range.

6. Conclusion.

The present study at high spatial resolution brings a direct experimental evidence of the existence of three different local structures observed in brine rich binary (surfactant/brine) or ternary (surfactant/alcohol/brine) phases namely spherical, cylindrical or planar. This confirms thoroughly our previous assumptions regarding these local structures which were derived, in particular, from experiments at low spatial resolution.

The best measure of the characteristic dimension (the radius of the sphere of the cylinder of the thickness of the bilayer) is obtained from the oscillations of the scattering pattern in the high q-range as expected [15]. The decrease of this characteristic dimension when going from the spherical to the planar structure is similar to that observed in concentrated mesophases in similar systems [27, 28]. This implies that the characteristic dimension in a particular local structure depends essentially on the geometry of the structure and not on the reasons which drive the system to adopt a given local structure (properties of the surfactant layer and/or interactions between aggregates).

The thickness of the bilayer ($d = 22$ Å) in the L_3 phase (deduced from the high spatial resolution measurements) is significantly different from that ($d = 26.5$ Å) in the adjacent lamellar phase L_α which was previously deduced from the evolution of the position of the Bragg peak of the lamellar phase with dilution [29]. This difference is possibly real however we feel that another explanation is more plausible namely that the thickness of the lamellae in the L_α phase (deduced in an indirect way) is artificially larger than the real thickness as a result of the large ondulations of the lamellae : $d_{\text{apparent}} = (S/S_p)\, d$ with S, the real surface of the lamella, and S_p, the projection of this surface on a plane perpendicular to the axis of the stack of lamellae. These ondulations have been evidenced by Electron Spin Resonance studies [30] on the same L_α phase. As noted above, they probably exist in the L_3 phase where they lead to the determination of apparently larger thicknesses in the low q-range (see above). A definitive answer to the questions, namely what is the real thickness in the L_α phase ? and is it equal to that of the L_3 phase ?, will be obtained from high spatial-resolution SANS we plan to make on L_α samples.

References

[1] PORTE G., APPELL J., *J. Phys. Chem.* **85** (1981) 2511.

[2] PORTE G., *J. Phys. Chem.* **87** (1983) 3541.

[3] YOUNG C. Y., MISSEL P. J., MAZER N. A., BENEDEK G. B., CAREY M. C., *J. Phys. Chem.* **82** (1978) 1375 ;
MISSEL P. J., MAZER N. A., BENEDEK G. B., YOUNG C. Y., CAREY M., *J. Phys. Chem.* **84** (1980) 1044.

[4] CANDAU S. J., HIRSCH E., ZANA R., *J. Phys. France* **45** (1984) 1263 ; *J. Colloid Interface Sci.* **105** (1985) 521 ; Physics of complex and supremolecular fluids, Eds. S. Safran and N. Clark (Wiley, New York) 1987, p. 569.

[5] CATES M. E., *Macromolecules* **20** (1987) 2289.

[6] CATES M. E., ROUX D., ANDELMAN D., MILNER S. T., SAFRAN S. A., *Europhys. Lett.* **5** (1988) 733.

[7] PORTE G., APPELL J., BASSEREAU P., MARIGNAN J., *J. Phys. France* **50** (1989) 1335.

[8] GOMATI R., APPELL J., BASSEREAU P., MARIGNAN J., PORTE G., *J. Phys. Chem.* **91** (1987) 6203.
[9] PORTE G., MARIGNAN J., BASSEREAU P., MAY R., *J. Phys. France* **49** (1988) 511.
[10] HOFFMANN H., SCHWANDNER B., ULBRICHT W., ZANA R., Physics of amphiphiles : Micelles, Vesicles and microemulsions, Eds. V. Degiorgio, M. Corti (North Holland, Amsterdam) 1985, p. 261.
[11] BENTON W. J., MILLER C. A., *J. Phys. Chem.* **87** (1983) 4891 ;
NATOLI J., BENTON W. J., MILLER C. A., FORD Jr T. J., *J. Dispersion Sci. Technol.* **7** (1986) 215.
[12] PORTE G., GOMATI R., EL HAITAMY O., APPELL J., MARIGNAN J., *J. Phys. Chem.* **90** (1986) 5746.
[13] GUINIER A., FOURNET G., Small angle Scattering of X-rays (Wiley, New York) 1955.
[14] GLATTER O., KRATKY O., Small angle X-rays Scattering (Academic Press, New York) 1982.
[15] CABANE B., DUPLESSIX R., ZEMB T., *J. Phys. France* **46** (1985) 2161 ;
CABANE B., Surfactant solutions, new methods of investigation, Ed. R. Zana (Marcel Dekker, New York) 1987, p. 57.
[16] JACROT B., ZACCAI G., *Biopolymers* **20** (1981) 2413.
[17] MAY R. P., IBEL K., HAAS J., *J. Appl. Cryst.* **15** (1982) 15.
[18] PORTE G., APPELL J., POGGI Y., *J. Phys. Chem.* **84** (1980) 3105.
[19] PORTE G., APPELL J., Surfactants in solution, Eds. K. L. Mittal, B. Lindman (Plenum Press, New York) **2** (1984) 1.
[20] LOVESEY S. W., Theory of neutron scattering from condensed matter (Clarendon Press, Oxford) 1986.
[21] CABANE B., DUPLESSIX R., ZEMB T., Surfactants in solution, Eds. K. L. Mittal and B. Lindman (Plenum Press, New York) 1984, p. 373.
[22] APPELL J., PORTE G., POGGI Y., *J. Colloid Interface Sci.* **87** (1982) 492.
[23] DEBYE P., *J. Phys. Colloid Chem.* **51** (1947) 18.
[24] KIRSTE R. G., OBERTHÜR R. C., Small angle X-rays Scattering, Eds. O. Glatter, O. Kratky (Academic Press, New York) 1982, p. 387.
[25] DES CLOIZEAUX J., Macromolecules **6** (1973) 403.
[26] DE GENNES P. G., Scaling concept in polymer physics (Cornell University Press G.B.) 1979.
[27] EKWALL P., Advances in Liquid Crystals, Ed. G. M. Brown (Academic Press, New York) 1975.
[28] SKOULIOS A., *Ann. Phys.* **3** (1978) 421.
[29] BASSEREAU P., MARIGNAN J., PORTE G., *J. Phys. France* **48** (1987) 673.
[30] DI MEGLIO J. M., BASSEREAU P., to be published.